The Astrophysical Journal Letters, 937:L39 (6pp), 2022 October 1 https://doi.org/10.3847/2041-8213/ac913d

Magnetic Switchbacks Heat the Solar Corona

M. Akhavan-Tafti[1], J. Kasper[1], J. Huang[1], and L. Thomas[2]
[1] University of Michigan, Ann Arbor, MI, USA; akhavant@umich.edu
[2] Washtenaw Community College, Ann Arbor, MI, USA
Received 2022 June 2; revised 2022 September 6; accepted 2022 September 12; published 2022 October 3

Abstract

Magnetic switchbacks are short magnetic field reversals ubiquitously observed in the solar wind. The origin of switchbacks remains an important open science question, because of switchbacks' possible role in the heating and acceleration of the solar wind. Here, we report observations of 501 robust switchbacks, using magnetic and plasma measurements from the first eight encounters by the Parker Solar Probe. More than 46% (6%) of switchbacks are rotational (tangential; TD) discontinuities (RD), defined as magnetic discontinuities with large (small) relative normal components of magnetic field and proton velocity. Magnetic reconnection in the solar atmosphere can be a source of the observed RD-type switchbacks. It is discovered that: (1) the RD-to-TD ratio exponentially decays with increasing heliocentric distance at rate 0.06 [R_S^{-1}], and (2) TD-type switchbacks contain 64% less magnetic energy than RD-type switchbacks, suggesting that RD-type switchbacks may relax into TD-type switchbacks. It is estimated that relaxing switchbacks generated via magnetic reconnection in the solar atmosphere can transfer an additional 16% of the total reconnected magnetic energy into heating and/or accelerating the solar corona, within 11.6 [R_S] of the reconnection site, below the critical Alfvén surface.

Unified Astronomy Thesaurus concepts: Solar coronal heating (1989); Solar magnetic reconnection (1504); Solar wind (1534); Heliosphere (711)

1. Introduction

The observation of patches of magnetic switchbacks in the young solar wind is one of the most notable discoveries (Bale et al. 2019; Kasper et al. 2019) of NASA's flagship Parker Solar Probe (PSP) mission. Magnetic switchbacks are short radial magnetic field reversals, ubiquitously observed in the solar wind. Observation of suprathermal electrons (Kahler et al. 1996), the differential streaming of alpha particles (Yamauchi et al. 2004) and proton beams (Neugebauer & Goldstein 2013), and the directionality of Alfvén waves (Balogh et al. 1999) suggest that switchbacks represent local folds in the magnetic field rather than changes in the magnetic connectivity to solar source regions.

The origin of switchbacks remains an important open science question. The primary motivation for understanding the origin of switchbacks is to understand their possible role in the heating and acceleration of the solar wind. The theories put forth to explain the origin of switchbacks can be divided into two main categories: (1) "ex situ" transient, impulsive processes, namely magnetic reconnection (Fisk & Kasper 2020; Drake et al. 2021), taking place in the solar atmosphere, and (2) "in situ" processes occurring locally within the solar wind, including those due to flow shear (Landi et al. 2006) and turbulence (Barnes & Hollweg 1974; Goldstein et al. 1974), as the solar wind propagates outwards.

Magnetic reconnection is a physical process that explosively converts magnetic energy into heat and kinetic energy. Solar flares are a result of magnetic reconnection, during which the stored magnetic energy (reaching up to 10^{26} Joules) is partly released as heat to increase the temperature of the plasma to a level when it emits X-rays (Yokoyama & Shibata 1995). The majority of coronal heating models invoke either dissipation of waves or magnetic reconnection (Parker 1988). Nevertheless, the relative importance of these two interdependent processes remains one of the outstanding unsolved problems in solar and astrophysics.

Here, we report observations of 501 robust switchbacks in the solar wind. The magnetic and plasma characteristics of these switchbacks are investigated to shed light on the generation mechanism(s) and the evolution of switchbacks.

2. Methods

In this study, the magnetic (Bale et al. 2016) and plasma (Kasper et al. 2016) measurements aboard PSP spacecraft are used from the first eight prehelion encounters. An automated algorithm, described in Akhavan-Tafti et al. (2021), is utilized to identify 3027 reversals in the radial component of magnetic field B_R in the first eight encounters. Minimum variance analysis (MVA) is performed on more than half of the identified B_R-reversals with clear magnetic field signatures (1884 quality events), defined as having five distinct regions, the leading quiet solar wind (QL), the leading transition region (TL), the spike region with a steady magnetic field (SPIKE), the trailing transition region (TT), and the trailing quiet solar wind (QT), as shown in Figure 1. The goal of the MVA analysis is to determine the switchback dimensionality, spatial orientation, and magnetic discontinuity categorization.

3. Results

Only 1390 of the 1884 quality switchbacks showed robust MVA results (Lepping & Behannon 1980), defined as having ratios of the intermediate-to-minimum eigenvalues $\lambda_2/\lambda_3 \geqslant 2.0$ at both the leading and trailing transition regions (Akhavan-Tafti et al. 2021). Next, 501 of the robust switchbacks containing quality plasma measurements within all five distinct regions are investigated. The transition regions are categorized

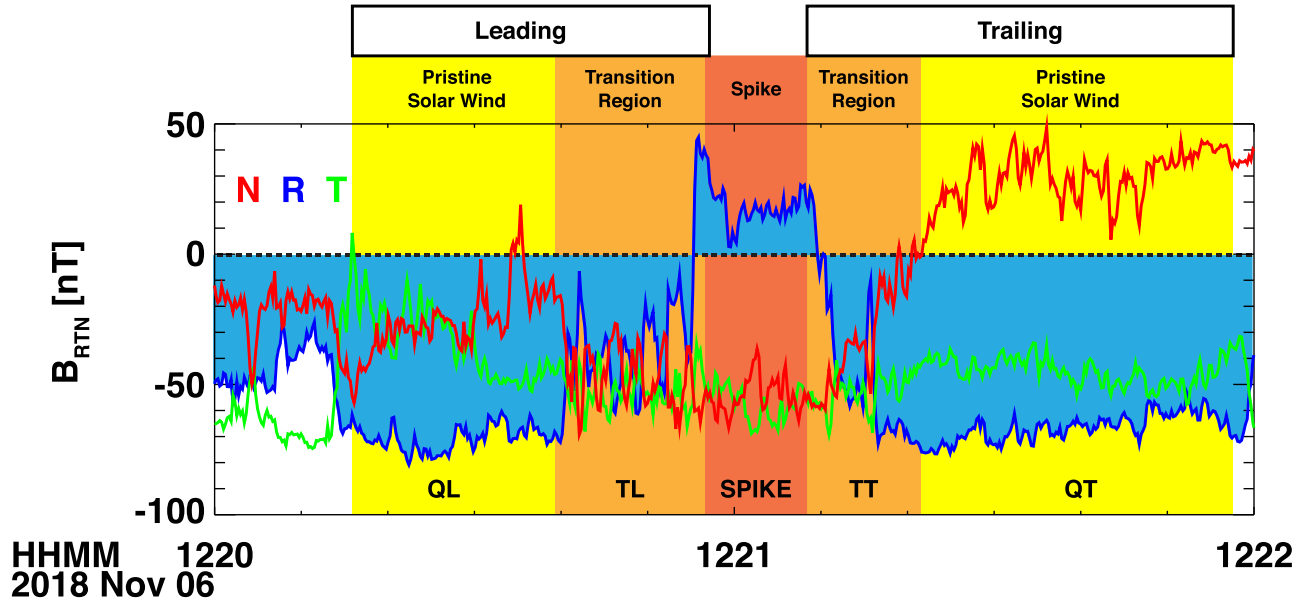

Figure 1. Magnetic field profile of a magnetic switchback event in rotational (R), tangential (T), and normal (N) coordinates during the first PSP encounter. A switchback comprises a magnetic spike that is separated from the pristine solar wind by a transition region. The radial component of the magnetic field reverses inside the transition region. The interval is 120 s in duration.

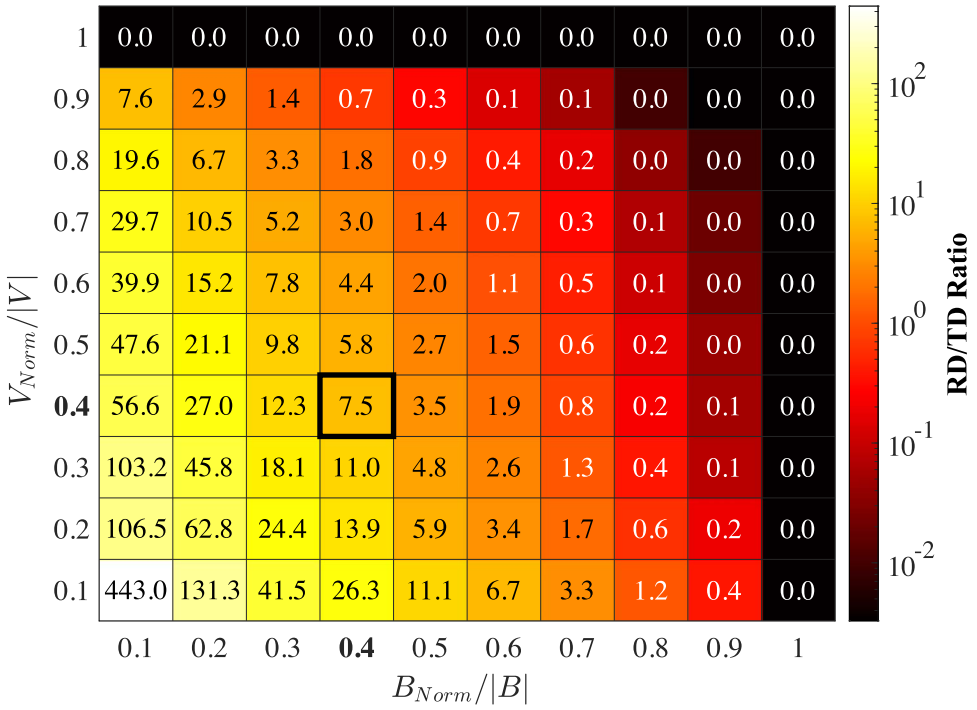

Figure 2. Heat map of the RD-to-TD boundary value, determined based on the relative magnitudes of the normal magnetic field and proton velocity across the leading switchback transition regions. The bold rectangle marks the RD-to-TD boundary value 0.4, below which both $|B_{\rm Norm}|/|B|$ and $|V_{\rm Norm}|/|V| < 0.4$.

based on their relative $B_{\rm Norm}$ and $V_{\rm Norm}$ across the leading switchback transition regions (Hudson 1970):

1. Rotational Discontinuity (RD): $|B_{\rm Norm}|/|B| \geqslant 0.4$ and $|V_{\rm Norm}|/|V| \geqslant 0.4$, and,
2. Tangential Discontinuity (TD): $|B_{\rm Norm}|/|B| < 0.4$ and $|V_{\rm Norm}|/|V| < 0.4$,

where $|B|$ and $|V|$ in the denominator are the larger of the magnetic field and proton velocity magnitudes on either side of the discontinuity. The discontinuity criteria are based on the fact that an RD-type magnetic discontinuity requires the transfer of momentum (non-negligible $V_{\rm Norm}$) across the boundary, in contrast with TD-type switchbacks.

The RD-to-TD boundary value 0.4 is selected according to Figure 2, which shows the significance of the choice of a boundary between RD- and TD-type switchbacks based on their relative magnitudes of the normal magnetic field and proton velocity across the leading switchback transition regions. For instance, the event counts for RD-to-TD boundary value 0.4 are RD:TD = 234:32, corresponding to RD-to-TD ratio = 7.5, averaged across all heliocentric distances.

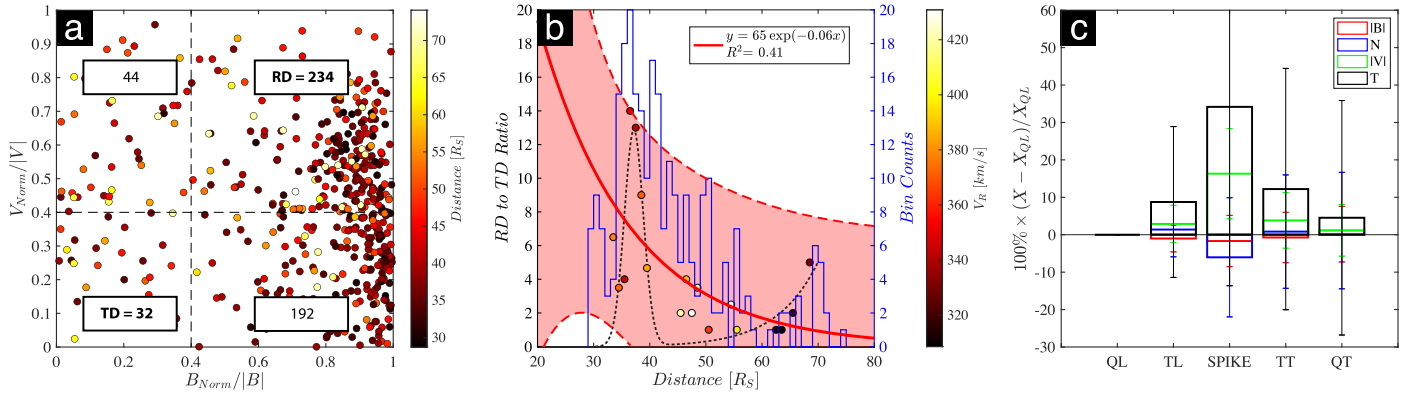

Figure 3. (a) Scatter plot of the relative magnitudes of the normal magnetic field and proton velocity across the leading switchback transition regions. The color bar represents the heliocentric distance of the observed switchback in solar radii [R_S]. (b) Scatter plot of RD-to-TD event count ratio as a function of heliocentric distance at the leading switchback transition regions. The color bar represents the average proton velocity in the leading quiet region. The blue histogram indicates the event count inside each distance bin (bin width = 1 R_S). The solid red curve represents the exponential fit, $y = a\ e^{-bx}$, where a and b are the y-intercept (at $x = 0$) and the decay rate in the unit [R_S^{-1}], respectively. The light red shaded region corresponds to the 95% confidence interval within which the observed RD-to-TD ratios within each radial bin may fall. The dashed black line denotes a two-term Gaussian model fit to the RD-to-TD data: $y = a_1 \exp(-((x-b_1)/c_1)^2) + a_2 \exp(-((x-b_2)/c_2)^2)$, where $a_1 = 12.88$, $b_1 = 37.11$, $c_1 = 2.454$, $a_2 = 8.0\text{e}^{+14}$, $b_2 = 554.9$, $c_2 = 84.8$. The correlation factor is $R^2 = 0.72$. (c) The superposed epoch analysis of $|B|$ (red), proton density N (blue), proton velocity $|V|$ (green), and proton radial temperature T (black) within the five distinct regions, relative to the leading quiet solar wind (QL). The error bars represent the standard deviation in each region.

Figure 3(a) shows that the leading switchback boundaries are dominantly RD-type magnetic discontinuities. Furthermore, it is indicated that the distribution of discontinuity types across the leading and trailing switchback transition regions is quite similar, RD:TD=234:32 at the leading transition regions and 239:35 at the trailing transition regions (not shown here).

Figure 3(b) shows a scatter plot of the RD-to-TD event count ratio as a function of heliocentric distance at the leading switchback transition regions. To distinguish between "ex situ" and "in situ" switchback generation mechanisms, two fits are investigated: (1) the red curve represents the exponential fit, $y = a\ e^{-bx}$, where a and b are the y-intercept and the exponential decay rate. It shows that with increasing heliocentric distance the number of RD-type switchback boundaries decreases rapidly relative to the number of TD-type discontinuities. The exponential fit also indicates that the leading switchback transition regions are dominantly RD-type at smaller heliocentric distances, in the solar corona, $a = 65$. The exponential decay rate at which the RD-type switchback transition regions become TD-type varies between the leading ($b = 0.06$ [R_S^{-1}]) and trailing ($b = 0.03$ [R_S^{-1}]) boundaries. In other words, the relative $B_{\rm Norm}$ decays with heliocentric distance at a rate that is twice as fast at the leading switchback transition regions than the trailing regions, and (2) the dashed black line further represents a two-term Gaussian fit to the RD-to-TD event count ratio. The fit indicates that the relative number of RD-type switchbacks peaks at 37.1 [R_S]. The bin counts and the fit further show that at smaller heliocentric distances the number of switchbacks, as well as the relative number of RD-type switchbacks, is sharply reduced.

Figure 3(c) shows the superposed epoch analysis of the 501 switchback events. In particular, the average jumps in different physical parameters relative to those at the leading quiet solar wind are determined $(X–X_{\rm QL})/X_{\rm QL}$, where X denotes physical parameters including $|B|$, proton number density N, proton speed $|V|$, and proton radial temperature T. The switchback spikes span between a few seconds to hundreds of minutes in duration, with a median of 52 s. The total event duration, including the quiet, transition, and spike regions, has a median of 207 s.

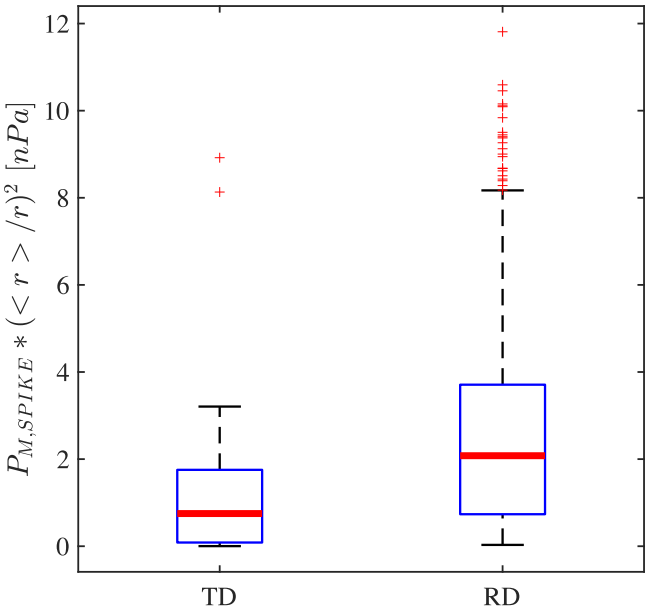

Figure 4. Boxplot of the normalized magnetic pressure, categorized based on switchback magnetic discontinuities. On each box, the red bar indicates the median, and the bottom and top edges of the blue box indicate the 25th and 75th percentiles, respectively. The whiskers extend to the most extreme data points not considered outliers, and the outliers are plotted individually using the "+" marker symbol.

It is found that on average (with large uncertainty): (1) $|B|$ is relatively unchanged across the leading and trailing transition regions, (2) $|N|$ reduces only slightly (by −9%) inside the spike region, (3) $|V|$ is 15% larger within the spike region than the surrounding solar wind, (4) compared to the quiet solar wind, proton radial temperature T is 10% larger within the leading and trailing transition regions and 25% larger inside the spike region.

Figure 4 shows a boxplot of the normalized magnetic pressure, categorized based on switchback magnetic discontinuity type. The normalization factor $(< r > /r)^2$ allows the comparison of magnetic pressure P_M inside switchback spike regions observed at various heliocentric distances, r. The parameter $< r >$ denotes the average heliocentric distance for

all switchback observations. It indicates that the median (red bar) normalized magnetic pressure P_M of TD-type (median = 0.75 [nPa]) switchbacks is 64% smaller than that of RD-type (median = 2.08 [nPa]) switchbacks. The difference is found to be statistically significant (probability $p > 0.95$).

4. Discussion and Conclusions

The magnetic and plasma characteristics of 501 switchback boundaries are investigated. The key results are:

1. More than 46% of the switchback boundaries are identified as having large relative discontinuity magnetic field and proton velocity normals $B_{\rm Norm}/|B| \geqslant 0.4$ and $V_{\rm Norm}/|V| \geqslant 0.4$, corresponding to RD-type magnetic discontinuities. Only 6% of the switchback events are categorized as TD-type discontinuities.
   (a) 192 or 38% of the switchbacks are categorized as having non-negligible (RD-type) relative normal magnetic field and negligible (TD-type) relative normal proton velocity. These Alfvénic discontinuities are likely of "incompressive" nature and prone to Kelvin–Helmholtz instability (Sen 1964; Burlaga 1969).
2. It is further shown that the switchback boundaries are dominantly RD-type at smaller heliocentric distances, suggesting that switchbacks are most likely generated via processes capable of producing RD-type magnetic structures.
   (a) One likely RD generation mechanism in the solar atmosphere is magnetic reconnection (Lee et al. 1996).
3. The relative number of RD-type switchbacks decreases with increasing heliocentric distance.
   (a) The exponential decay rate may indicate that RD-type switchbacks evolve into magnetic discontinuities with smaller discontinuity normal angles; that is, TD-type, with increasing heliocentric distance.
   (b) In contrast, the peak at 37.1 [R_S] in the relative number of RD-type switchbacks may indicate that switchbacks are generated via "in situ" processes in the solar wind. The peak, however, may be a result of insufficient event counts at smaller heliocentric distances.
   (c) It is also possible that the TD-type switchbacks are generated via processes that are different from those of RD-type switchbacks. One such process includes the nonlinear evolution of Alfvén waves in the solar wind (Cohen & Kulsrud 1974).
   (d) The observed exponential decay may also suggest the merging (Akhavan-Tafti et al. 2018) and clustering of switchbacks into switchback patches (Kasper et al. 2019), defined as bundles of switchbacks with relatively small discontinuity normal (TD-type).
4. Switchbacks comprise five distinct regions –the spike region being separated from the surrounding quiet solar wind by leading and trailing transition regions. It is found (with large uncertainties) that, compared to the surrounding quiet solar wind, proton velocity (+15%) and radial temperature (+25%) sharply increase at the switchback spikes, while the magnetic field remains continuous (−2%) and proton density (−9%) only slightly decreases, in agreement with Farrell et al. (2020).
   (a) These characteristics may indicate that the plasma contained within switchbacks is either from a source region with faster and hotter plasma than the quiet solar wind or that the frozen-in plasma is accelerated and heated as the switchbacks propagate away from the Sun. Alternatively, as proposed by Matteini et al. (2014), the enhancement in proton velocity inside the spike region is a result of the Alfvenic nature of switchbacks. Additionally, the significant enhancement in proton radial temperature at the spike region is proposed to be a result of the rotation of a fixed anisotropic temperature (Woolley et al. 2020).
5. It is further shown that RD-type switchback transition regions have greater magnetic ($U_B \propto P_M$) energy than TD-type switchbacks, suggesting that RD-type switchbacks generated on the Sun may relax into magnetic discontinuities with smaller discontinuity normal angles as they propagate away from the Sun. The relaxed, TD-type magnetic switchbacks are characterized as having 64% smaller magnetic energy ($U_{B,\rm relaxation} = P_{M,\rm TD}/P_{M,\rm RD} = 0.64$). The kinetic ($U_E \propto P_{\rm TH}$) and bulk flow energy ($U_F \propto P_{\rm Dyn}$) of plasmas within switchbacks are also found (not shown here) to be smaller for the TD-type switchbacks.
   (a) It is determined that the exponential decay rate at which RD-type switchbacks likely evolve into switchbacks with smaller discontinuity normal angles is between 3×10^{-2} and 6×10^{-2} [R_S^{-1}]. At this rate, relaxing RD-type switchbacks generated in the solar atmosphere will deposit half (half-life: $x_{1/2} = -\ln(1/2)/b$) of their magnetic energy into the surrounding ambient plasma within $x_{1/2} = 11.6$–23.1 [R_S] of generation. Therefore, this relaxation can heat the solar corona by 32% of the total switchback magnetic energy ($U_{B,\rm relaxation}/U_{B,\rm out} = 0.32$), assuming switchbacks contain all of the magnetic energy released in the reconnection outflow region ($U_{B,\rm out}$).

   Previous studies (in collisionless plasmas) have shown that nearly half of the magnetic energy flowing into a reconnection region ($U_{\rm tot,in}$) is converted to particle energy. The other half of $U_{\rm tot,in}$ is released as magnetic energy ($U_{B,\rm out}/U_{\rm tot,in} = 0.5$) in the reconnection outflow region (Yamada et al. 2018). This indicates that more than 16% of the total reconnected magnetic energy ($U_{\rm B,relaxation}/U_{\rm tot,in} = 0.16$) is deposited into the ambient plasma by the observed relaxing RD-type switchbacks far from the reconnection site.

   For scale comparison, the ion inertial length ($r_i \propto N$) in the low-beta solar corona is of the order of few tenths of one meter, $r_i \ll x_{1/2}$, indicating that the magnetic energy deposited into heating the solar corona takes place far from the reconnection outflow region ($x_{1/2} \sim 10^{10}\ r_i$). Similar nonlocal impacts of magnetic reconnection have been reported in other low-beta plasma environments, including the Earth's magnetosphere using in situ measurements from NASA's flagship Magnetospheric Multiscale (MMS) mission (Akhavan-Tafti et al. 2019b; Akhavan-Tafti et al. 2020).

To summarize, Figure 5 shows our proposed mechanisms responsible for the generation and evolution of magnetic switchbacks, based on (1) the exponential decay fit to the relative RD-type switchback counts with heliocentric distance, and (2) the substantial difference in the magnetic pressure of RD- and TD-type switchbacks. It is proposed that an RD-type

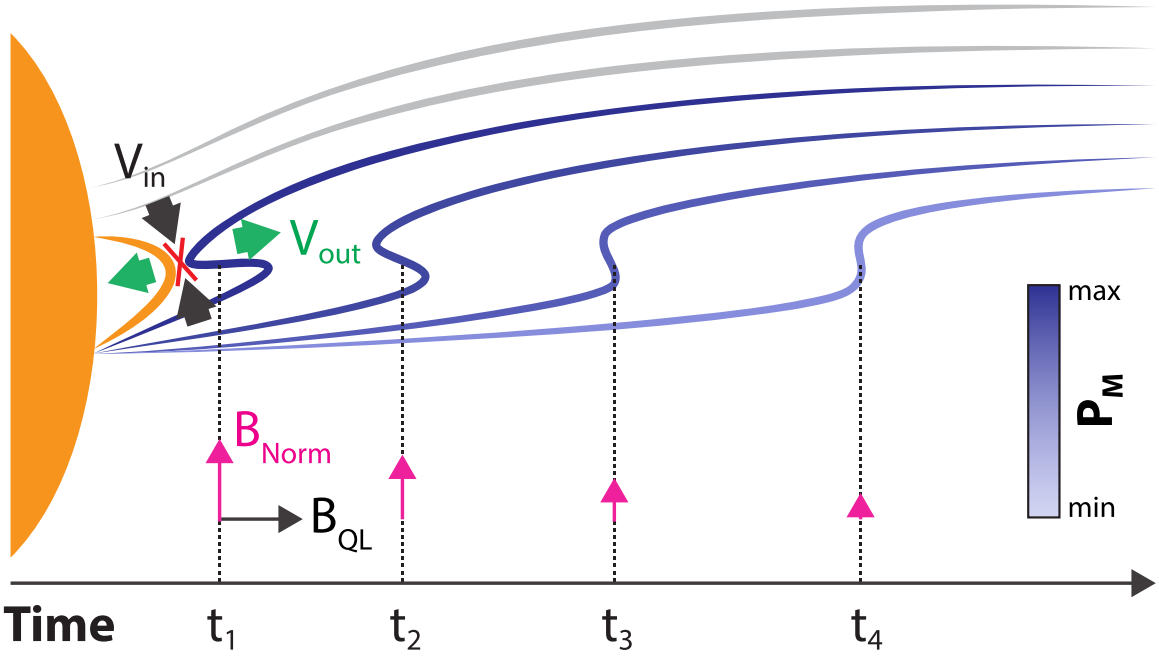

Figure 5. Concept illustration of the generation mechanism and temporal evolution of a magnetic switchback (dark blue). Magnetic reconnection between closed coronal loops (orange line) and open field lines (gray line) is shown by a red cross. The reconnection inflow (V_{in}) and outflow (V_{out}) regions are marked by black and green arrows, respectively. The magenta arrows indicate the magnitude of B_{Norm} relative to B_{QL}. The shade of blue indicates magnetic pressure (P_M) at the switchback spike region.

switchback is generated in the solar atmosphere via magnetic reconnection (an "ex situ" process) between closed coronal magnetic loops and open field lines (Zank et al. 2020). Therefore, the characteristics of the switchback, including the thickness of the spike region and the rate of evolution, should depend on the properties of the source magnetic reconnection. It is believed that, over time, the relative magnitude of B_{Norm} is reduced, resulting in the switchback becoming a magnetic discontinuity with a relatively small discontinuity normal. Therefore, it is estimated that this RD-to-TD switchback evolution can release up to 16% of the total switchback magnetic energy into the solar corona, likely within the critical Alfvén surface ($x_{1/2} = 11.6$–23.1 [R_S]). It is further estimated that relaxing switchbacks can heat and/or accelerate the solar corona plasma by $\Delta P_{RT}/x_{1/2} = 4.4\ \mathrm{J\ m^{-2}}$, where $\Delta P_{RT} = 0.5 \times (P_{RD}\text{-}P_{TD}) = 0.73$ nPa. In other words, a relaxing switchback of area $A = D^2 = 100\ \mathrm{Mm^2}$, where D is assumed to be the length scale of a small solar coronal flare (Ni et al. 2020), can contribute 4.4×10^{14} J (or 120 GWh) to the coronal plasma energy budget.

Caveat: The proposed mechanisms are based on the exponential decay fit to the relative RD-type switchback counts with heliocentric distance. Considering the observed peak in the relative number of RD-type switchbacks, one may conclude that switchbacks may be generated via "in situ" processes. Alternatively, the observed peak may be a result of "ex situ" generated switchbacks evolving through various processes and/or at different rates.

The mechanisms through which RD-type switchbacks may relax and the corresponding processes to dissipate this released magnetic energy, including waves (Mozer et al. 2020) and/or turbulence, remain open science questions. It is also important to investigate whether and how switchbacks within the critical Alfvén layer are different from those observed farther from the Sun. Future PSP and Solar Orbiter encounters and global simulations will shed further light onto the generation and evolution of magnetic switchbacks and help advance our understanding of our star.

The authors are grateful for the dedicated efforts of the PSP team. This work was supported by NASA contract Nos. NNN06AA01C, 80NSSC20K1847, 80NSSC20K1014, and 80NSSC21K1662. The authors would also like to thank Aditya Gandhi at the University of Michigan for help with data analysis.

ORCID iDs

M. Akhavan-Tafti https://orcid.org/0000-0003-3721-2114
J. Kasper https://orcid.org/0000-0002-7077-930X
J. Huang https://orcid.org/0000-0002-9954-4707
L. Thomas https://orcid.org/0000-0002-2589-8166

References

Akhavan-Tafti, M., Fontaine, D., Slavin, J. A., Le Contel, O., & Turner, D. 2020, JGRA, 125, e2020JA028027
Akhavan-Tafti, M., Kasper, J., Huang, J., & Bale, S. 2021, A&A, 650, A4
Akhavan-Tafti, M., Slavin, J. A., Le, G., et al. 2018, JGRA, 123, 1224
Akhavan-Tafti, M., Slavin, J. A., Sun, W. J., Le, G., & Gershman, D. J. 2019, GeoRL, 46, 654
Bale, S. D., Badman, S. T., Bonnell, J. W., et al. 2019, Natur, 576, 237
Bale, S. D., Goetz, K., Harvey, P. R., et al. 2016, SSRv, 204, 49
Balogh, A., Forsyth, R. J., Lucek, E. A., Horbury, T. S., & Smith, E. J. 1999, GeoRL, 26, 631
Barnes, A., & Hollweg, J. V. 1974, JGR, 79, 2302
Burlaga, L. F. 1969, SoPh, 7, 72
Cohen, R. H., & Kulsrud, R. M. 1974, PhFl, 17, 2215
Drake, J. F., Agapitov, O., Swisdak, M., et al. 2021, A&A, 650, A2
Farrell, W. M., MacDowall, R. J., Gruesbeck, J. R., Bale, S. D., & Kasper, J. C. 2020, ApJS, 249, 28
Fisk, L. A., & Kasper, J. C. 2020, ApJL, 894, L4
Goldstein, M. L., Klimas, A. J., & Barish, F. D. 1974, Solar Wind Three On the Theory of Large Amplitude Alfven Waves, Goddard Space Flight Center,

https://ntrs.nasa.gov/api/citations/19740014712/downloads/19740014712.pdf
Hudson, P. D. 1970, P&SS, 18, 1611
Kahler, S. W., Crooker, N. U., & Gosling, J. T. 1996, JGR, 101, 24373
Kasper, J. C., Abiad, R., Austin, G., et al. 2016, SSRv, 204, 131
Kasper, J. C., Bale, S. D., Belcher, J. W., et al. 2019, Natur, 576, 228
Landi, S., Hellinger, P., & Velli, M. 2006, GeoRL, 33, L14101
Lee, L. C., Lin, Y., & Choe, G. S. 1996, SoPh, 163, 335
Lepping, R. P., & Behannon, K. W. 1980, JGRA, 85, 4695
Matteini, L., Horbury, T. S., Neugebauer, M., & Goldstein, B. E. 2014, GeoRL, 41, 259
Mozer, F. S., Agapitov, O. V., Bale, S. D., et al. 2020, ApJS, 246, 68
Neugebauer, M., & Goldstein, B. E. 2013, in AIP Conf. Proc. 1539, Proc. of the Thirteenth International Solar Wind Conf. (Melville, NY: AIP), 46
Ni, L., Ji, H., Murphy, N. A., & Jara-Almonte, J. 2020, RSPSA, 476, 20190867
Parker, E. N. 1988, ApJ, 330, 474
Sen, A. K. 1964, PhFl, 7, 1293
Woolley, T., Matteini, L., Horbury, T. S., et al. 2020, MNRAS, 498, 5524
Yamada, M., Chen, L. -J., Yoo, J., et al. 2018, NatCo, 9, 5223
Yamauchi, Y., Suess, S. T., Steinberg, J. T., & Sakurai, T. 2004, JGRA, 109, A03104
Yokoyama, T., & Shibata, K. 1995, Natur, 375, 42
Zank, G. P., Nakanotani, M., Zhao, L. L., Adhikari, L., & Kasper, J. 2020, ApJ, 903, 1